Talanta 149 (2016) 237–243

Contents lists available at ScienceDirect

Talanta

journal homepage: www.elsevier.com/locate/talanta

Rapid three-dimensional microfluidic mixer for high viscosity solutions to unravel earlier folding kinetics of G-quadruplex under molecular crowding conditions

Chao Liu, Ying Li, Yiwei Li, Peng Chen, Xiaojun Feng, Wei Du, Bi-Feng Liu *

Britton Chance Center for Biomedical Photonics at Wuhan National Laboratory for Optoelectronics – Hubei Bioinformatics & Molecular Imaging Key Laboratory, Systems Biology Theme, Department of Biomedical Engineering, College of Life Science and Technology, Huazhong University of Science and Technology, Wuhan 430074, China

ARTICLE INFO

Article history:
Received 23 September 2015
Received in revised form
11 November 2015
Accepted 16 November 2015
Available online 17 November 2015

Keywords:
Microfluidic chip
Micromixer
Folding kinetics
G-quadruplex

ABSTRACT

Rapid mixing of highly viscous solutions is a great challenge, which helps to analyze the reaction kinetics in viscous liquid phase, particularly to discover the folding kinetics of macromolecules under molecular crowding conditions mimicking the conditions inside cells. Here, we demonstrated a novel microfluidic mixer based on Dean flows with three-dimensional (3D) microchannel configuration for fast mixing of high-viscosity fluids. The main structure contained three consecutive subunits, each consisting of a "U"-type channel followed by a chamber with different width and height. Thus, the two solutions injected from the two inlets would undergo a mixing in the first "U"-type channel due to the Dean flow effect, and simultaneous vortices expansions in both horizontal and vertical directions in the following chamber. Numerical simulations and experimental characterizations confirmed that the micromixer could achieve a mixing time of 122.4 μs for solutions with viscosities about 33.6 times that of pure water. It was the fastest micromixer for high viscosity solutions compared with previous reports. With this highly efficient 3D microfluidic mixer, we further characterized the early folding kinetics of human telomere G-quadruplex under molecular crowding conditions, and unravelled a new folding process within 550 μs.

1. Introduction

G-quadruplexes are abundant in eukaryotic telomeres and some promoter regions [1–4], which are unique four-stranded structures formed by guanine-rich nucleic acids through Hoogsteen hydrogen bonding [5]. There are growing evidences suggesting that such structures might participate in DNA replication, [6] transcription [7,8] and immunoglobin switching [9]. For example, the folding and formation of human G-quadruplexes (d$(TTAGGG)_4$) structures play significant roles in the aging processes and the formation of cancer [10]. The theoretical model of G-quadruplexes predicted a complex folding process in dilute solutions, [11] which have been experimentally confirmed with stopped flow and microfluidic mixer [12–14]. Gray et al. utilized three sequence variants to demonstrate that DNA quadruplexes fold into compact structures by following a multistep pathway [15]. However, the actual folding process of G-quadruplex happens in a molecular crowding environment in vivo, which might modify the structures of G-quadruplex and influence its folding mechanism [5,16–19]. By using viscous polyethylene glycol (PEG) solutions to mimic the intracellular environment, scientists have investigated the structures and thermodynamics of G-quadruplexes in molecular crowding conditions [20–23]. It was reported that the human telomerase sequence forms antiparallel-stranded G-quadruplexes in diluted aqueous solution but a parallel-stranded structure in the molecular crowding condition [17,24]. However, little was known about the early folding kinetics of G-quadruplexes in molecular crowding condition that is crucial for understanding its folding mechanism due to the lack of ultrafast mixing approach for highly viscous solutions.

Rapid mixing has been recognized as an attractive approach to analyze the chemical kinetics of fast reactions [25]. Traditionally, stopped-flow instruments have provided valuable information on the mechanisms of protein and DNA folding [26,27]. However, the millisecond-scale dead time precluded us from conducting a detail analysis of the early folding events [28]. Previous literatures have demonstrated the study of folding kinetics by coupling microfluidic mixers with various detection methods such as Förster resonance energy transfer (FRET) [29], small-angle X-ray scattering (SAXS) [30], circular dichroism (CD)[31] and Raman spectroscopy [32]. Microfluidics-based technologies have accomplished

* Correspondence to: Department of Biomedical Engineering College of Life Science and Technology Huazhong University of Science and Technology, Wuhan 430074, China.
E-mail address: bfliu@mail.hust.edu.cn (B.-F. Liu).

http://dx.doi.org/10.1016/j.talanta.2015.11.036
0039-9140/

significant improvements in mixing dead time and sample consumption [33]. As the Reynolds number (Re) is usually low in microfluidic chip, the mixing in the channel primarily depends upon molecular diffusion [34]. In the case of passive mixers two mixing concepts have been employed to create a mixed flow, [35] the lamination method simply using molecular diffusion for mixing that is not suited for mixing high-viscosity solutions, [36] and the chaotic method using flow advection for mixing. Several attempts to generate chaotic advection in microfluidic mixers by building ribs, grooves or other structures in microchannels, or placing obstacles in the flow path, [37–42] but few of them have demonstrated the ability to mix high-viscosity fluids. Recently, active microfluidic mixers were developed for mixing high viscous fluids of low Re by oscillating bubbles, about 100 ms of mixing dead time could be achieved [43,44].

We previously developed a ω-shaped baffles passive micromixer achieving a mixing time of 579.4 μs for solutions with viscosities about 33.6 times that of pure water, which led a discovery of the early folding kinetics of d(TTAGGG)$_4$ in crowding solutions at 1 ms [45]. However, no earlier folding process could be found hiding in the mixing dead time. In this paper, we proposed a new three dimensional (3D) passive multivortex microfluidic mixer based on Dean flows and expansion vortices in horizontal and vertical. The mixing performances of the devices were firstly visualized through mixing deionized water and various concentrations of PEG200 in numerical simulations and experimental evaluation. It was demonstrated the 3D micromixer could mix solutions with viscosity of up to 35.25 mPa s in 122.4 μs representing an improvement about 1000-fold in mixing dead time compared with active micromixers. With this highly efficient 3D micromixer, we observed a unique folding kinetics of human telomere G-quadruplex under molecular crowding conditions within 150–550 μs.

2. Experimental

2.1. Materials and sample preparations

Chemicals such as fluorescein, sulforhodamine B, 1-anilion-8-naphthalene-sulfonic acid (ANS), bovine serum albumin (BSA), methanol, PEG200, EGTA, Tris, HCl, and NaOH were purchased from Sinopharm Chemical Reagent (Shanghai, China). The oligonucleotide (d(TTAGGG)$_4$) purchased from TaKaRa Biotech (Dalian, China) was labeled with 5′-fluorescein (FAM) and 3′-tetramethylrhodamine (TMR) and further purified by high-performance liquid chromatography. Various concentrations of PEG200 were prepared in TE buffer (10 mM Tris, 1 mM EDTA, pH 7.3). Sulforhodamine B was dissolved in TE buffer with a concentration of 1 μM. Fluorescein was dissolved in methanol and diluted in various PEG200 solutions with a final concentration of 1.0 μM. The oligonucleotide solution (1.0 μM, diluted in TE buffer) was heated to 95 °C for 5 min and was slowly cooled to room temperature (20 °C) before analysis. All solutions were prepared with deionized water (Millipore, Bedford, MA, USA).

2.2. Optical imaging system and operation procedures

Experiments were carried out on a laser scanning confocal microscope (LSCM) system (FV1000, Olympus, Japan). An Argon laser (λ=488 nm) and a He–Ne laser (λ=543 nm) were used as excitation light. Using an objective of 10× (NA 0.3), fluorescein (sulforhodamine B) solution was excited with 488 nm (543 nm) light; the emission fluorescence was collected from 510 to 550 nm (575–615 nm). With the same objective, the double-labeled oligonucleotide solution was excited with 488 nm light, and the emission fluorescence was collected at 510–550 nm for FAM and 575–615 for TMR. The spatial resolution along the z-axis was 1 μm and the exposure time of each pixel was 8 μs. Acquired images were further analyzed using software Image Pro Plus 6.0 (Media Cybernetics, Bethesda, MD). To get an identical volumetric flow rate, a syringe pump (Scientific, USA) was used to inject solutions into the two inlets of the micromixer.

2.3. Numerical simulation

All the simulations were carried out by using the simulation software Fluent 6.1 (Fluent Inc., Lebanon, NH, USA). In a 3D finite volume model, the simulations of both 2D micromixer and 3D micromixer have been conducted for a comparison. The continuity equation, the Navier–Stokes equation, and the diffusion–convection equation have been solved in the simulation. Pure water and various concentrations of PEG200 were injected to the inlets respectively at the rate of 0.21 mL/min. The properties of the solutions were the same as previously described by Li et al. [45].

2.4. Chip fabrication

Mixers were fabricated by using the standard soft-lithography technique as previously reported [46]. Briefly, The master mold for the 3D microstructure was produced by consecutively coating a silicon wafer n-type (100) with 17 μm and 34 μm thick layers of negative photoresist SU-8 1700 (Gersteltec Sarl, Switzerland), exposing the photoresist through two separate photomasks. The cast of poly (dimethylsiloxane) (PDMS) made from a mixture of 10:1 (m/m) PDMS and curing agent (Sylgard 184, Dow Corning, USA) was obtained by molding the SU-8 structure. To reduce the deformability of the PDMS, the cast of PDMS with a thickness of about 100 μm was irreversibly bonded between a cover slide and a glass slide with holes drilled by a numerically controlled machine.

3. Results and discussion

3.1. Design of micromixer

Fluids traveling through curvilinear channels experience an inter-play between inertial forces acting to direct axial motion and centrifugal effects acting along the conduit's radius of curvature [47]. “Dean number” κ [$\kappa=(d/R)^{0.5}$Re, d is the channel hydraulic diameter, R is the flow path radius of curvature, Re is Reynolds number [48]] accounts for the relative magnitude of inertial and centrifugal to viscous forces. When the Dean number is large enough, centrifugal effects will be strong enough to perturb the axial laminar flow profile, causing two parallel fluid streams to switch position. On the other hand, fluid encountering a sudden increase in a conduit's cross-sectional area undergoes local separation from the wall in response to adverse pressure gradient in the formation of a vortex pair breaking the entrance to expansion [49]. Based on Dean flows effects, a multivortex mixer with the action of expansion vortices in horizontal (two dimensional, 2D) has been developed by Sudarsan and Ugaz [47].

Theoretically, 3D mode would have a better performance for liquids mixing than 2D mode as the enhanced chaotic advection in microchannel [50–53]. In this regard, we designed the passive multivortex micromixer as shown in Fig. 1. The main structure was a “T”-type configuration, in which three consecutive subunits were embedded at the stem area. Each subunit was consisted of a “U”-type channel followed by a chamber with different width and height than the “U”-type channel. Thus, the two solutions injected

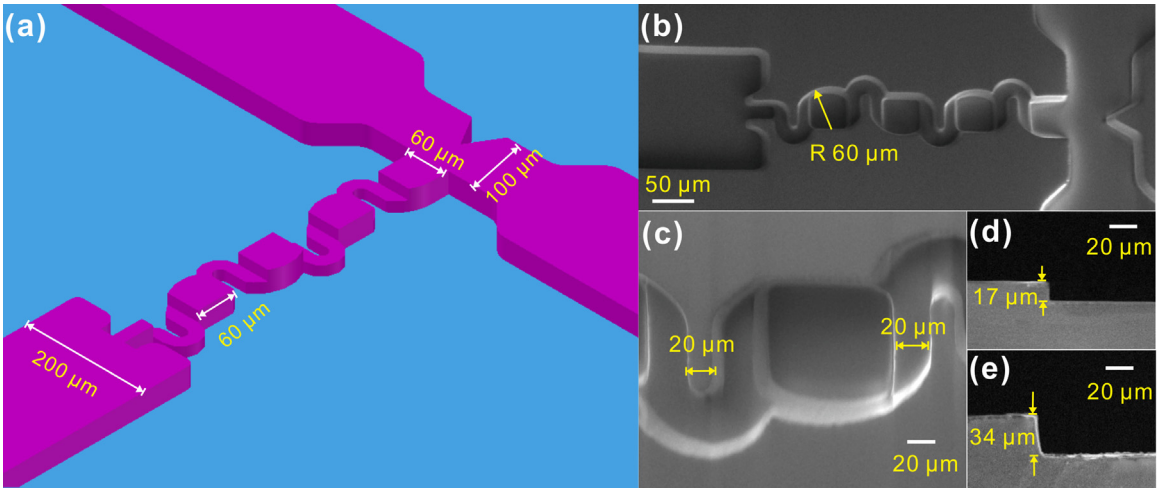

Fig. 1. Schematic of the 3D micromixer. (a) The mixer consists of two inlets, injection channels, mixing section, and out channels. The widths of the main channel and the "U"-type channel were 200 μm and 20 μm, the chamber had a length of 60 μm. (b) SEM image of the microchannel. (c) SEM image of the detail mixing units. (d) and (e) The vertical cross-sectional views of the microchannel. The heights of the "U"-type channel and the chamber were 17 μm and 34 μm, respectively. The total volume of the mixing part is 0.857 nL.

from the two inlets would undergo a mixing in the first "U"-type channel due to the Dean flow effect. Such mixing would be further enhanced in the following chamber because of simultaneous vortices expansions in both horizontal and vertical directions. After this process was repeated for three times, the mixed solution was then introduced into an observation channel for analysis. To demonstrate a better mixing performance of the 3D micromixer than 2D format, we also fabricated a 2D micromixer sharing the same chip configuration as the 3D micromixer but with the same height at all regions of chip microchannel.

3.2. Computational fluid dynamics (CFD) simulation

For evaluating the mixing behavior inside the mixing microchannel, CFD simulations were conducted by mixing pure water and various concentrations of PEG200. As shown in Fig. 2a, solutions of pure water and 80% (w/v) PEG200 were injected at the flow rate of 0.21 mL/min from two inlets, flowed through three consecutive subunits for mixing and reached the final observation region. For quantitative evaluating the mixing performance, the mixing efficiency of the two mixers were calculated (The equation

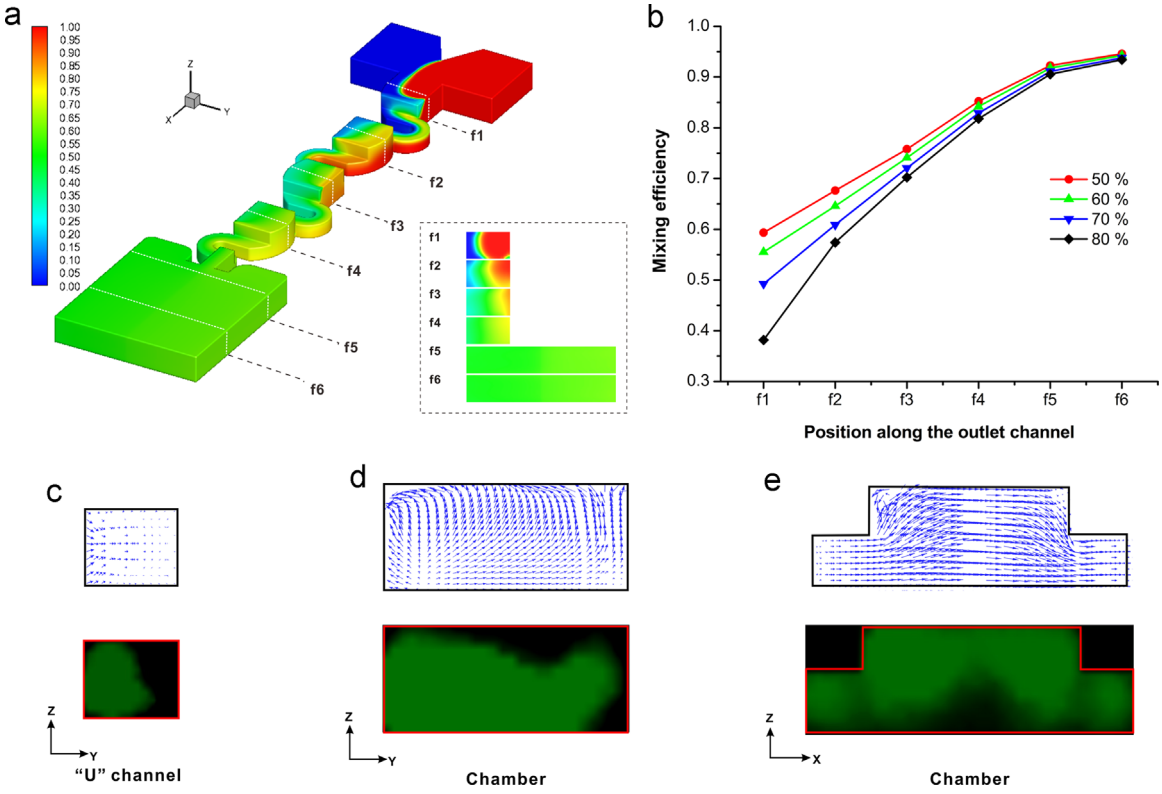

Fig. 2. Mixing results of the 3D micromixer. (a) Simulated species mass fraction contours of mixing pure water and 80% PEG200 respectively at flow rate of 0.21 mL/min (Re= 9.86).The inset shown the vertical cross-sectional simulation results at f1–f6. (b) Simulated results of mixing efficiency of pure water and various concentrations of PEG200 at f1–f6. (c) The numerical simulation and experimental results of Dean flow in the "U" type channel. The fluid has been transported from the inter wall (left wall) to the outer wall (right well). (d, e) The numerical simulation and experimental results of expansion vortices in the 3D chamber at y–z plane (d) and x–z plane (e).

is shown in supporting information). Fig. 2b showed the mixing efficiency (C_m) of water with various concentrations of PEG200 (50%, 60%, 70%, and 80%) at given positions (from f1 to f6) with the flow rate of 0.21 mL/min. Obviously, lower concentration of PEG200 representing lower fluid viscosity had better mixing efficiency at all the check points. However, the water with the highest concentration PEG200 (80%) still had a mixing efficiency above 0.9 (the number indicating a completing mixing [54]) at the position f5 (the entrance of the observation channel), which largely proved that the configuration design of this 3D micromixer was successful. As a comparison, CFD simulations of the 2D micromixer were also performed (Fig. S1). It was quite clear that 3D chip had much better performance than that of 2D chip in term of the mixing efficiency.

To a better understanding of the mechanism, the velocity vector distribution in microchannels was examined (Fig. 2c–e). It was found that the fluid has been transported from the inner wall toward the outer wall in the "U"-type channel, due to the effect of Dean flows. At the 3D chamber, simultaneous vortices expansions in both horizontal and vertical directions happened, which led to more significant vortex fluid, thus to achieve better fluids mixing. However, the expansion vortices of 2D mixer was created only in horizontal plane (Fig. S1).

3.3. Experimental evidence of mixing performance and dead time

The mixing performance of 3D micromixer were experimentally examined using TE buffer and various concentrations of PEG200 solutions at different flow rates. For visualization, sulforhodamine B and fluorescein as fluorescent indicators were added into the TE buffer and PEG200 solution (0%, 50%, and 80%) at the final concentration of 1 μM, respectively. The flow rates were varied from 0.005 mL/min to 0.21 mL/min for the optimization. With laser confocal fluorescence imaging, the Dean flow in the "U"-type channel (κ=9.2, for 40 % PEG200 solution at the total flow rate of 0.42 mL/min) and the expansion vortices in the chamber were visualized. Fig. 3a–d showed examples of the mixing TE buffer with 80% PEG200 solution at flow rate of 0.005, 0.05, 0.15 and 0.21 mL/min. It was clear that completed mixing only happened at the flow rate of 0.21 mL/min by investigating the confocal *x*–*y* image of the middle fluidic layer in observation channel, which was confirmed by fluorescent distribution at the check position f5 as described in Fig. 3f. The mixing conditions at *Z*-axis direction (cross-section *y*–*z* panel) at the entrance of the observation channel (check position f5) were also given in Fig. 3a–d. It further proved that the mixed solution in the observation region was homogeneous. Fig. 3e showed the fluorescent profiles at different check points (f1–f5) at the flow rate of 0.21 mL/min. It was found that the homogeneity level was increased while the solution passed through more microstructures for mixing. As a comparison shown in Fig. S2, the mixing efficiency of 3D micromixer was much better than that of 2D one. Further, we found the vertical cross-sectional fluorescence distribution at f1–f5 fit well with the simulation results in Fig. S3.

It was not surprised that the mixing performance increased as the flow rate increased as shown in Fig. 4, because of larger Re would enhance the Dean flow and the Chaos in mixing region. For the 80% PEG200 solution, when the flow rate was increased to 0.21 mL/min, the mixing efficiency was calculated to be 0.91 (above 0.9) in check position f5, which meant complete mixing. We calculated the dead time by simply dividing the volume of the mixing part (0.857 nL) by total flow velocity (0.42 mL/min) [39]. The result was 122.4 μs, about 5-fold improvement compared with our previous report.

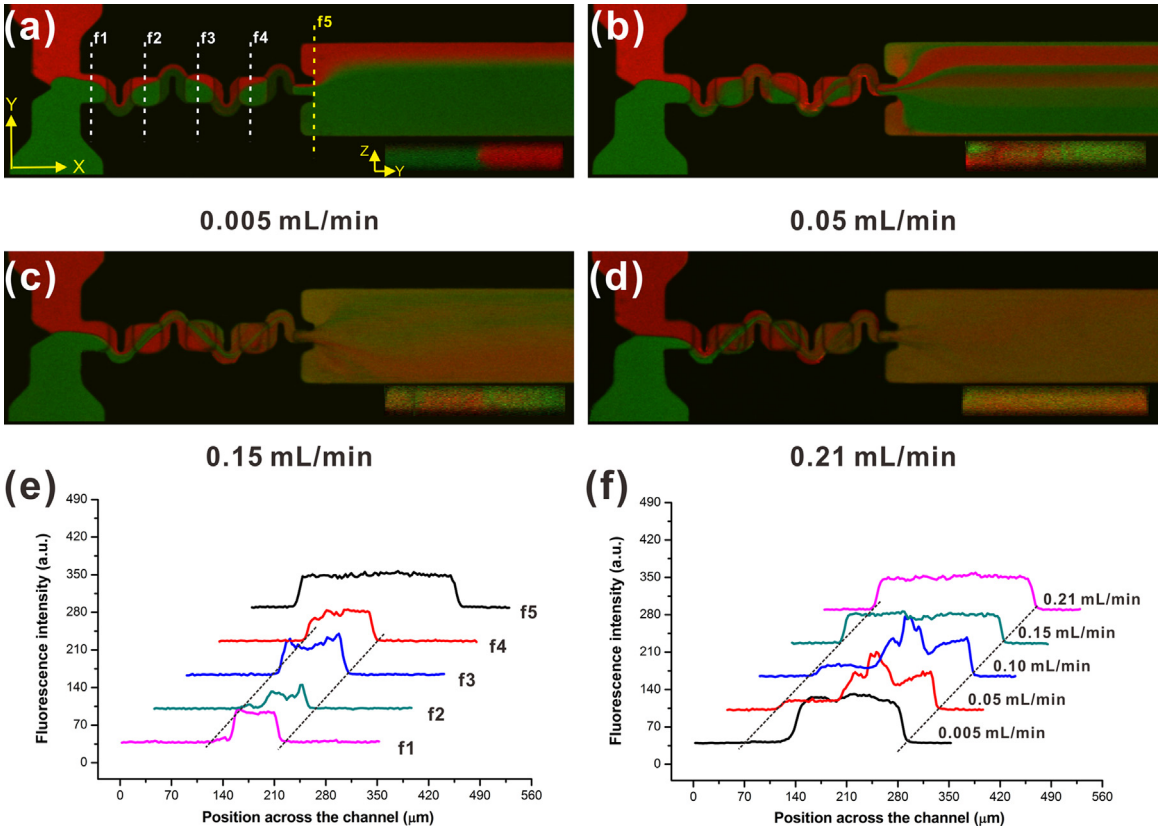

Fig. 3. Mixing performance of buffer and 80% PEG200. (a–d) Fluorescence distribution of middle layer given by LSCM along the *Z*-axis at flow rates of (a) 0.005, (b) 0.10, (c) 0.15, (d) 0.21 mL/min. The insets are the fluorescence distribution of cross sections at position f5. (e) Fluorescence distribution across the channel at position f1–f5 at the flow rate of 0.21 mL/min. (f) Fluorescence distribution across the channel at position f5 under various flow rates.

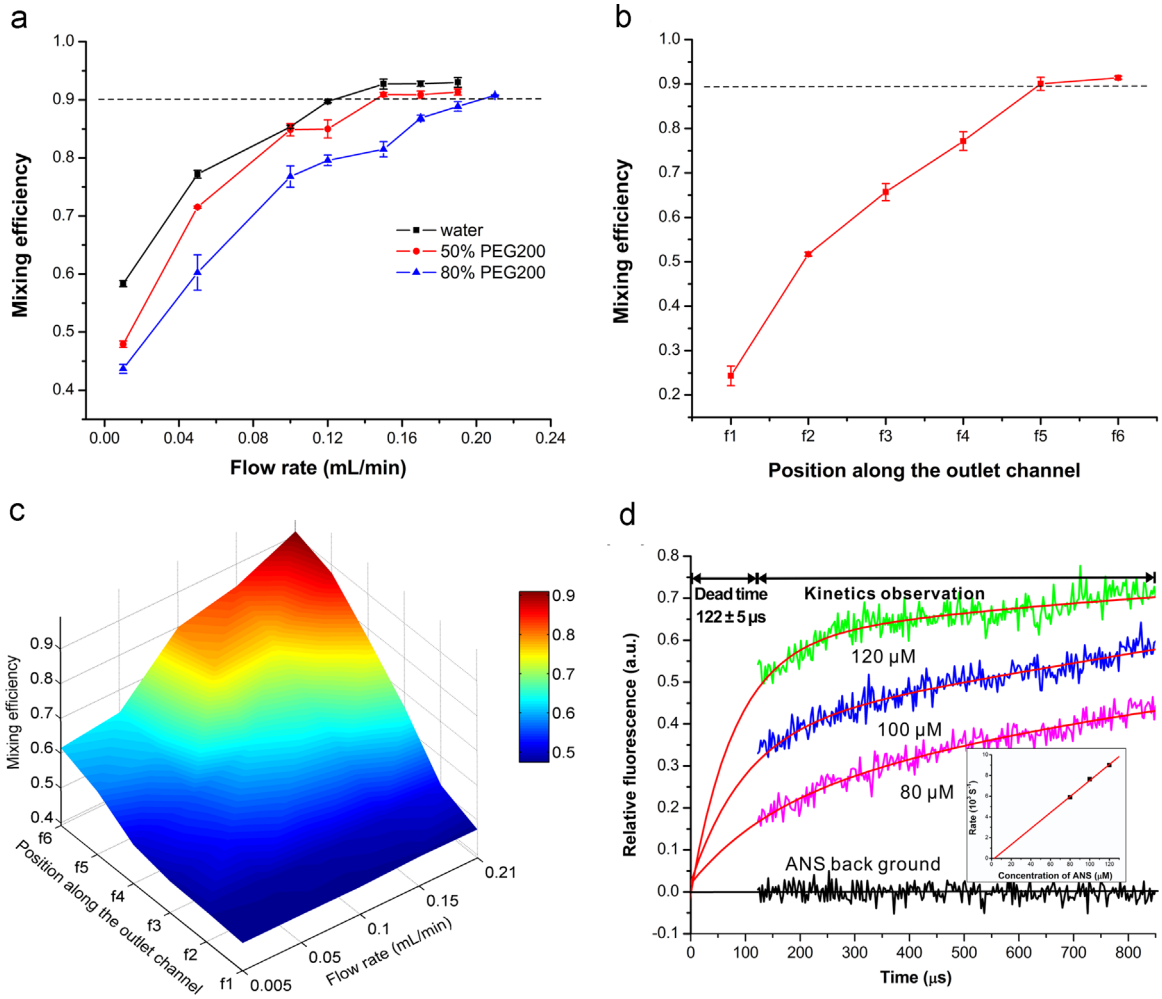

Fig. 4. Evaluation of mixing efficiency and confirmation of the dead time. (a) Mixing efficiency of various concentrations of PEG200 under various flow rates at position f5. (b) Mixing efficiency of buffer and 80% PEG200 at position of f1–f6 at the flow rate of 0.21 mL/min. (c) Surface plot of mixing efficiency of buffer and 80% PEG200 as a function of flow rate and position along the outlet channel. (d) Confirmation of the dead time by using the chemical reaction of ANS binding to the protein BSA. The intensity changes were fitted by double exponentials. The inset is measured rate constants of faster phase plotted as a function of concentration of ANS. The corresponding second-order rate constant is $(8.847 \pm 0.356) \times 10^7\ M^{-1}\ s^{-1}$.

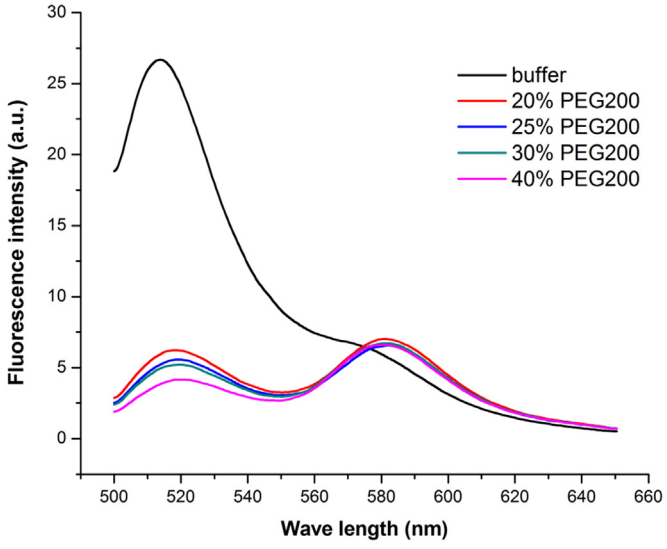

Fig. 5. Fluorescence spectroscopy of the double-labeled G-quadruplex under various concentrations of PEG200.

The dead time was also validated by using a chemical reaction of ANS binding to the protein BSA (Fig. 4d). The 7.0 μM BSA solution and various concentrations (80 μM, 100 μM, and 120 μM) of ANS solutions were injected to the 3D mixer at the flow rate of 0.21 mL/min, respectively. We measured the fluorescence intensity changes after mixing the BSA solution (pH 7.0). The fitted lines for different ANS concentrations intersected at the time representing the initiation point of mixing, and the time delay from this point to the first observable point corresponds to the dead time is 122 ± 5 μs [55]. The apparent rate constants for the binding reaction plotted as the function of the ANS concentration was linear.

3.4. Folding kinetics of G-quadruplex

Our previous work has investigated the folding kinetics of G-quadruplex under molecular crowding conditions in a unique microfluidic mixer with a mixing time of 579.4 μs, and observed the exponential process at the time of ~1000 μs. However, little was known in the hidden mixing dead time. In this work, further attempt was tried to unravel the much earlier folding kinetics of G-quadruplex with the new 3D micromixer.

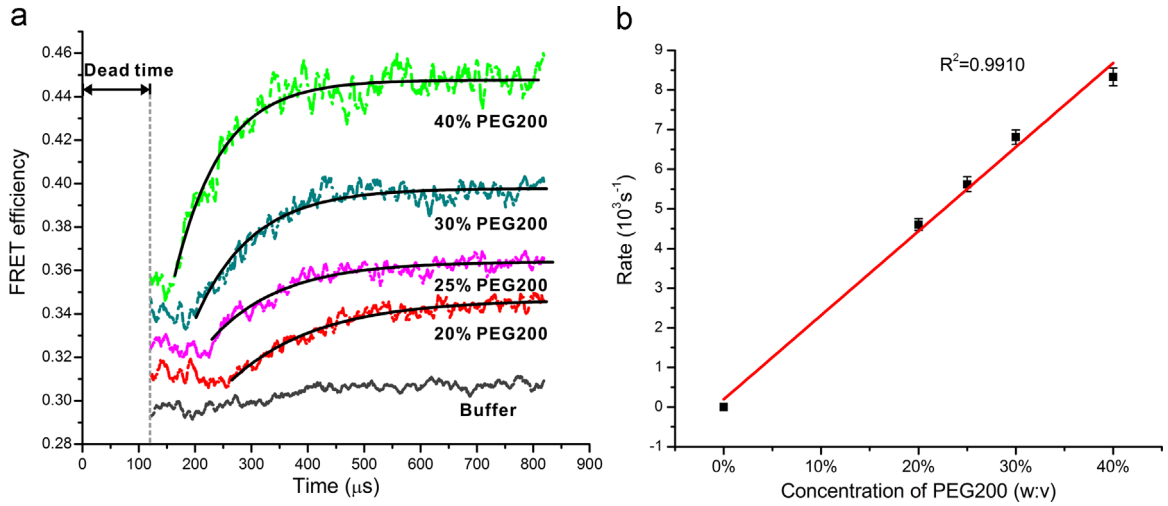

Fig. 6. Folding kinetics analysis for human telomere G-quadruplex monitored by FRET efficiency in the observe channel. (a) The FRET efficiency of double-labeled G-quadruplex measured at the observation channel of the 3D mixer by LSCM. Labeled G-quadruplex solution was rapid mixing into a buffer solution and into final crowding conditions of 20%, 25%, 30% and 40% PEG200, respectively. The lines are single-exponential fits of the date. (b) The apparent rate constants of the refolding as the function of the PEG200 concentration. The observed kinetics in 20%, 25%, 30% and 40% were $(4.604 \pm 0.146) \times 10^3$, $(5.620 \pm 0.189) \times 10^3$, $(6.813 \pm 0.180) \times 10^3$, and $(8.327 \pm 0.225) \times 10^3\ s^{-1}$, respectively.

The G-quadruplex folding reaction was initiated by fast mixing 1.0 μM oligonucleotide d(TTAGGG)$_4$ with 40%, 50%, 60%, and 80% (w/v) concentrations of PEG200 to a final PEG200 concentrations of 20%, 25%, 30% and 40% at the flow rate of 0.21 mL/min, respectively. We also tested the refolding of G-quadruplex in reaction tubes to verify the results observed on the microchip as shown in Fig. 5. The images of fluorescence intensities of the acceptor and the donor labeled at the two ends (3′ and 5′) of oligonucleotide were then simultaneously recorded by LSCM in the observation channel. The fluorescence resonance energy transfer (FRET) efficiency expressed as proximity ratio $I[(I=I_a/(I_a+I_d))$, I_a and I_d are the fluorescence intensities of the acceptor and donor, respectively [56].] reveals the conformational changes of the oligonucleotide. The kinetic measurement stated from the entrance of the observation channel corresponding to 122.4 μs (the dead time). It was interesting that an exponential rise phase were discovered in the time window of 150–550 μs as shown in Fig. 6, which was certainly beyond the measurement capability of any reported micromixer. The folding process could be fitted by single exponentials as expected for the pseudo-first-order kinetics, which was certainly beyond the measurement capability of any reported micromixer. We calculated the folding kinetics in 20%, 25%, 30% and 40% PEG200 solutions. The apparent rate constants for the reaction plotted as the function of the PEG200 concentration was linear. In our new 3D mixer, we also found an exponential rise phase at the time of ~1000 μs as shown in Fig. S4, which has been reported in our previous work. As a control experiment, G-quadruplex solution was also mixed with TE buffer solution. No folding signal was found. Therefore, we found there were two steps in the folding kinetic process of G-quadruplex under molecular crowding conditions, which was consistent with the hypothetical folding pathway in dilute solutions [12,14].

As a comparison, we further investigated the folding kinetics of human telomeric DNA of d[AGGG(TTAGGG)$_3$] (Tel22) in high viscosity solutions (Fig. S5). Deleting TT from 5′ of the sequence increased the folding rate in high viscosity solutions, which was consistent with previous study (Fig. S6) [15]. We believe this 3D micromixer was a powerful approach for tracking rapid conformational changes of biological macromolecules under molecular crowding conditions.

4. Conclusions

We have proposed a novel 3D micromixer based on Dean flow coupling with 3D expansion vortices for rapid mixing highly viscous solutions. The fluids mixing efficiency was validated by both numerical simulation and experimental evaluation. It proved that the pure water and 80% PEG200 (with viscosities about 33.6 times that of pure water) could be completed mixed in 122.4 μs. With this micromixer, we observed a new folding kinetic process of G-quadruplex within 550 μs. We believed that this micromixer would also be useful tool for the analysis of biomacromolecules folding kinetics such as nucleic acids or proteins under molecular crowding conditions. Finally, it should be pointed out that the theoretical modeling is also crucial. The entire folding kinetics has been revealed for G-quadruplex in diluted solution. The theoretical model predicted every intermediate process, which was then confirmed by experimental evidence. With more and more experimental clues were discovered for the G-quadruplex in molecular crowding conditions, a new theoretical model was highly desired.

Acknowledgements

We gratefully acknowledge the financial supports from National Natural Science Foundation of China (21475049, 31471257 and 21275060) and National Basic Research Program of China (2011CB910403).

Appendix A. Supplementary material

Supplementary data associated with this article can be found in the online version at http://dx.doi.org/10.1016/j.talanta.2015.11.036.

References

[1] R.K. Moyzis, J.M. Buckingham, L.S. Cram, M. Dani, L.L. Deaven, M.D. Jones, J. Meyne, R.L. Ratliff, J.R. Wu, A highly conserved repetitive DNA sequence, (TTAGGG)n, present at the telomeres of human chromosomes, Proc. Natl.

Acad. Sci. USA 85 (1988) 6622–6626.
[2] E.H. Blackburn, Structure and function of telomeres, Nature 350 (1991) 569–573.
[3] T. Simonsson, G-quadruplex DNA structures–variations on a theme, Biol. Chem. 382 (2001) 621–628.
[4] Y. Xu, X. Feng, W. Du, X. Liu, Q. Luo, B.F. Liu, Kinetic and thermodynamic characterization of telomeric G-quadruplex by nonequilibrium capillary electrophoresis: application to G-quadruplex/duplex competition, Anal. Chem. 80 (2008) 6935–6941.
[5] D. Miyoshi, A. Nakao, N. Sugimoto, Molecular crowding regulates the structural switch of the DNA G-quadruplex, Biochemistry 41 (2002) 15017–15024.
[6] S.N. Saldanha, L.G. Andrews, T.O. Tollefsbol, Assessment of telomere length and factors that contribute to its stability, Eur. J. Biochem. 270 (2003) 389–403.
[7] J.L. Huppert, S. Balasubramanian, G-quadruplexes in promoters throughout the human genome, Nucleic Acids Res. 35 (2007) 406–413.
[8] T. Simonsson, P. Pecinka, M. Kubista, DNA tetraplex formation in the control region of c-myc, Nucleic Acids Res. 26 (1998) 1167–1172.
[9] M.L. Duquette, P. Handa, J.A. Vincent, A.F. Taylor, N. Maizels, Intracellular transcription of G-rich DNAs induces formation of G-loops, novel structures containing G4 DNA, Genes Dev. 18 (2004) 1618–1629.
[10] N. Jing, Y. Li, W. Xiong, W. Sha, L. Jing, D.J. Tweardy, G-quartet oligonucleotides: a new class of signal transducer and activator of transcription 3 inhibitors that suppresses growth of prostate and breast tumors through induction of apoptosis, Cancer Res. 64 (2004) 6603–6609.
[11] P. Stadlbauer, L. Trantirek, T.E. Cheatham, J. Koca, J. Sponer, Triplex intermediates in folding of human telomeric quadruplexes probed by microsecond-scale molecular dynamics simulations, Biochimie 105C (2014) 22–35.
[12] R.D. Gray, J.B. Chaires, Kinetics and mechanism of K+- and Na+-induced folding of models of human telomeric DNA into G-quadruplex structures, Nucleic Acids Res. 36 (2008) 4191–4203.
[13] A.Y. Zhang, S. Balasubramanian, The kinetics and folding pathways of intramolecular G-quadruplex nucleic acids, J. Am. Chem. Soc. 134 (2012) 19297–19308.
[14] Y. Li, C. Liu, X. Feng, Y. Xu, B.F. Liu, Ultrafast Microfluidic Mixer for Tracking the Early Folding Kinetics of Human Telomere G-Quadruplex, Anal. Chem. 86 (2014) 43334339.
[15] R.D. Gray, J.O. Trent, J.B. Chaires, Folding and unfolding pathways of the human telomeric G-quadruplex, J. Mol. Biol. 426 (2014) 1629–1650.
[16] D. Miyoshi, N. Sugimoto, Molecular crowding effects on structure and stability of DNA, Biochimie 90 (2008) 1040–1051.
[17] F.M. Lannan, I. Mamajanov, N.V. Hud, Human telomere sequence DNA in water-free and high-viscosity solvents: G-quadruplex folding governed by Kramers rate theory, J. Am. Chem. Soc. 134 (2012) 15324–15330.
[18] S. Nagatoishi, Y. Tanaka, K. Tsumoto, Circular dichroism spectra demonstrate formation of the thrombin-binding DNA aptamer G-quadruplex under stabilizing-cation-deficient conditions, Biochem. Biophys. Res. Commun. 352 (2007) 812–817.
[19] Z.Y. Kan, Y.A. Yao, P. Wang, X.H. Li, Y.H. Hao, Z. Tan, Molecular crowding induces telomere G-quadruplex formation under salt-dericient conditions and enhances its competition with duplex formation, Angew. Chem. Int. Ed. 45 (2006) 1629–1632.
[20] B. Heddi, A.T. Phan, Structure of human telomeric DNA in crowded solution, J. Am. Chem. Soc. 133 (2011) 9824–9833.
[21] D. Miyoshi, H. Karimata, N. Sugimoto, Hydration regulates thermodynamics of G-quadruplex formation under molecular crowding conditions, J. Am. Chem. Soc. 128 (2006) 7957–7963.
[22] J. Zhou, C.Y. Wei, G.Q. Jia, X.L. Wang, Q. Tang, Z.C. Feng, C. Li, The structural transition and compaction of human telomeric G-quadruplex induced by excluded volume effect under cation-deficient conditions, Biophys. Chem. 136 (2008) 124–127.
[23] R. Buscaglia, M.C. Miller, W.L. Dean, R.D. Gray, A.N. Lane, J.O. Trent, J.B. Chaires, Polyethylene glycol binding alters human telomere G-quadruplex structure by conformational selection, Nuleic. Acids. Res. 41 (2013) 7934–7946.
[24] J. Li, J.J. Correia, L. Wang, J.O. Trent, J.B. Chaires, Not so crystal clear: the structure of the human telomere G-quadruplex in solution differs from that present in a crystal, Nucleic. Acids Res. 33 (2005) 4649–4659.
[25] D.E. Hertzog, B. Ivorra, B. Mohammadi, O. Bakajin, J.G. Santiago, Optimization of a Microfluidic Mixer for Studying Protein Folding Kinetics, Anal. Chem. 78 (2006) 42994306.
[26] T. Kiefhaber, Kinetic traps in lysozyme folding, Proc. Natl. Acad. Sci. USA 92 (1995) 9029–9033.
[27] R.K. Nayak, O.B. Peersen, K.B. Hall, A. Van Orden, Millisecond time-scale folding and unfolding of DNA hairpins using rapid-mixing stopped-flow kinetics, J. Am. Chem. Soc. 134 (2012) 2453–2456.
[28] H. Roder, K. Maki, H. Cheng, Early events in protein folding explored by rapid mixing methods, Chem. Rev. 106 (2006) 1836–1861.
[29] L. Jiang, Y. Zeng, Q. Sun, Y. Sun, Z. Guo, J.Y. Qu, S. Yao, Microsecond protein folding events revealed by time-resolved fluorescence resonance energy transfer in a microfluidic mixer, Anal. Chem. 87 (2015) 5589–5595.
[30] L. Pollack, M.W. Tate, N.C. Darnton, J.B. Knight, S.M. Gruner, W.A. Eaton, R. H. Austin, Compactness of the denatured state of a fast-folding protein measured by submillisecond small-angle x-ray scattering, Proc. Natl. Acad. Sci. USA 96 (1999) 10115–10117.
[31] A.S. Kane, A. Hoffmann, P. Baumgartel, R. Seckler, G. Reichardt, D.A. Horsley, B. Schuler, O. Bakajin, Microfluidic mixers for the investigation of rapid protein folding kinetics using synchrotron radiation circular dichroism spectroscopy, Anal. Chem. 80 (2008) 9534–9541.
[32] S.I. Masca, I.R. Rodriguez-Mendieta, C.T. Friel, S.E. Radford, D.A. Smith, Detailed evaluation of the performance of microfluidic T mixers using fluorescence and ultraviolet resonance Raman spectroscopy, Rev. Sci. Instrum. 77 (2006) 055105.
[33] G.M. Whitesides, The origins and the future of microfluidics, Nature 442 (2006) 368–373.
[34] D.J. Beebe, G.A. Mensing, G.M. Walker, Physics and applications of microfluidics in biology, Annu. Rev. Biomed. Eng. 4 (2002) 261–286.
[35] N.T. Nguyen, Z.G. Wu, Micromixers – a review, J. Micromech. Microeng. 15 (2005) R1–R16.
[36] Y. Li, F. Xu, C. Liu, Y.Z. Xu, X.J. Feng, B.F. Liu, A novel microfluidic mixer based on dual-hydrodynamic focusing for interrogating the kinetics of DNA-protein interaction, Analyst 138 (2013) 4475–4482.
[37] T.J. Johnson, D. Ross, L.E. Locascio, Rapid microfluidic mixing, Anal. Chem. 74 (2002) 45–51.
[38] A.D. Stroock, S.K.W. Dertinger, A. Ajdari, I. Mezic, H.A. Stone, G.M. Whitesides, Chaotic mixer for microchannels, Science 295 (2002) 647–651.
[39] S. Matsumoto, A. Yane, S. Nakashima, M. Hashida, M. Fujita, Y. Goto, S. Takahashi, A. Rapid Flow, Mixer with 11-μs Mixing time microfabricated by a pulsed-laser ablation technique: observation of a barrier-limited collapse in cytochrome c folding, J. Am. Chem. Soc. 129 (2007) 38403841.
[40] K.P. Nichols, J.R. Ferullo, A.J. Baeumner, Recirculating, passive micromixer with a novel sawtooth structure, Lab. Chip 6 (2006) 242–246.
[41] D.J. Kim, H.J. Oh, T.H. Park, J.B. Choo, S.H. Lee, An easily integrative and efficient micromixer and its application to the spectroscopic detection of glucose-catalyst reactions, Analyst 130 (2005) 293–298.
[42] Y. Li, D.L. Zhang, X.J. Feng, Y.Z. Xu, B.F. Liu, A microsecond microfluidic mixer for characterizing fast biochemical reactions, Talanta 88 (2012) 175–180.
[43] S.S. Wang, X.Y. Huang, C. Yang, Mixing enhancement for high viscous fluids in a microfluidic chamber, Lab. Chip 11 (2011) 2081–2087.
[44] A. Ozcelik, D. Ahmed, Y. Xie, N. Nama, Z. Qu, A.A. Nawaz, T.J. Huang, An acoustofluidic micromixer via bubble inception and cavitation from microchannel sidewalls, Anal. Chem. 86 (2014) 5083–5088.
[45] Y. Li, Y. Xu, X. Feng, B.F. Liu, A rapid microfluidic mixer for high-viscosity fluids to track ultrafast early folding kinetics of G-quadruplex under molecular crowding conditions, Anal. Chem. 84 (2012) 9025–9032.
[46] D.C. Duffy, J.C. McDonald, O.J. Schueller, G.M. Whitesides, Rapid Prototyping of Microfluidic Systems in Poly(dimethylsiloxane), Anal. Chem. 70 (1998) 4974–4984.
[47] A.P. Sudarsan, V.M. Ugaz, Multivortex micromixing, Proc. Natl. Acad. Sci. USA 103 (2006) 7228–7233.
[48] S.A. Berger, L. Talbot, L.S. Yao, Flow in curved pipes, Annu. Rev. Fluid Mech. 15 (1983) 461–512.
[49] N. Alleborn, K. Nandakumar, H. Raszillier, F. Durst, Further contributions on the two-dimensional flow in a sudden expansion, J. Fluid Mech. 330 (1997) 169–188.
[50] D. Therriault, S.R. White, J.A. Lewis, Chaotic mixing in three-dimensional microvascular networks fabricated by direct-write assembly, Nat. Mater. 2 (2003) 265–271.
[51] D.S. Kim, S.H. Lee, T.H. Kwon, C.H. Ahn, A serpentine laminating micromixer combining splitting/recombination and advection, Lab. Chip 5 (2005) 739–747.
[52] T. Yasui, Y. Omoto, K. Osato, N. Kaji, N. Suzuki, T. Naito, M. Watanabe, Y. Okamoto, M. Tokeshi, E. Shamoto, Y. Baba, Microfluidic baker's transformation device for three-dimensional rapid mixing, Lab. Chip 11 (2011) 3356–3360.
[53] X. Feng, Y. Ren, H. Jiang, Effect of the crossing-structure sequence on mixing performance within three-dimensional micromixers, Biomicrofluidics 8 (2014) 34106.
[54] T. Egawa, J.L. Durand, E.Y. Hayden, D.L. Rousseau, S.R. Yeh, Design and evaluation of a passive alcove-based microfluidic mixer, Anal. Chem. 81 (2009) 1622–1627.
[55] M.C.R. Shastry, S.D. Luck, H. Roder, A continuous-flow capillary mixing method to monitor reactions on the microsecond time scale, Biophys. J. 74 (1998) 2714–2721.
[56] J.J. Green, L. Ying, D. Klenerman, S. Balasubramanian, Kinetics of unfolding the human telomeric DNA quadruplex using a PNA trap, J. Am. Chem. Soc. 125 (2003) 3763–3767.